Thin Solid Films 518 (2010) 6984–6992

Contents lists available at ScienceDirect

Thin Solid Films

journal homepage: www.elsevier.com/locate/tsf

Influences of roll-to-roll process and polymer substrate anisotropies on the tensile failure of thin oxide films

Yves Leterrier *[,a], Albert Pinyol [a], Luc Rougier [a], Judith H. Waller [a], Jan-Anders Månson [a], Pierre J.J. Dumont [b], Jānis Andersons [c], Jānis Modniks [c], Manuel Campo [d], Peter Sauer [d], Julian Schwenzel [d]

[a] Laboratoire de Technologie des Composites et Polymères (LTC), Ecole Polytechnique Fédérale de Lausanne (EPFL), Station 12, Lausanne CH-1015, Switzerland
[b] Laboratoire de Génie des Procédés Papetiers (LGP2), CNRS/Institut Polytechnique de Grenoble (Grenoble INP), 461 rue de la Papeterie, 38402 Saint-Martin-d'Hères, France
[c] Institute of Polymer Mechanics, 23 Aizkraukles Iela, Riga LV-1006, Latvia
[d] Applied Materials GmbH & Co. KG, Siemensstr. 100, D-63755 Alzenau, Germany

ARTICLE INFO

Article history:
Received 29 April 2009
Received in revised form 21 June 2010
Accepted 8 July 2010
Available online 16 July 2010

Keywords:
Anisotropy
Roll-to-roll processing
Failure
Internal stresses
Polymer substrates

ABSTRACT

The influence of internal stress anisotropy resulting from anisotropic loading in a roll-to-roll (R2R) process, and polymer substrate anisotropy on the crack onset strain (COS) of thin oxide coatings was analyzed. Experimental data obtained for R2R processed films were compared with data obtained using an isotropic sheet-to-sheet (S2S) process with the same anisotropic substrate. In the R2R case the COS was found to increase by 20% between the transverse direction and the machine direction. In the S2S case the COS was found to be independent of orientation, except at a 45° in-plane orientation with respect to the machine direction, where it was 15% higher. The internal stress in the machine direction could not be determined, presumably due to deposition-induced curvature changes of the polymer substrate, and was therefore fitted to the COS data. Fracture mechanics analysis and finite element modeling of the experimental data showed that the influence of substrate anisotropy was marginal, and that it was the process-induced internal strain in the coating which controlled the COS.

1. Introduction

Flexible electronic devices including displays and photovoltaic cells are currently being developed using polymer substrates [1–4]. Such devices present advantages, such as conformability and light weight, and are potentially compatible with cost-effective roll-to-roll (R2R) production processes [5]. These advantages may be compromised by the high levels of thermo-mechanical stresses often present in R2R processing, and the associated risk of mechanical failure of the fragile devices [6,7]. R2R processes are anisotropic in nature, the thin polymer foil being loaded along the so-called 'machine direction' to keep it flat during layer deposition [8]. The polymer foil itself, supplied in the form of a roll, is produced by means of extrusion casting followed by sequential biaxial stretching, and it is usually orthotropic [9–11]. The combination of substrate anisotropy and process anisotropy is expected to give rise to an anisotropic state of stress in deposited layers, hence to anisotropic fracture properties of the layers. The case in which channeling cracks occur through coating layers deposited on anisotropic substrates was treated in [12–15]. The reciprocal situation where channeling cracks develop through an anisotropic coating deposited on an isotropic substrate was investigated in [16]. In this case the coating anisotropy led to markedly different tensile failure strains, as well as to very different calculated coating energy release rates for both tested directions. Thus it would be useful to better understand anisotropic related issues, hence to identify the limits and develop a stable R2R process.

The objective of the work was to investigate the details of cracking anisotropy in relation to process-induced internal stress anisotropy and substrate anisotropy. The critical strain for tensile failure (crack onset strain, COS) of a thin oxide layer deposited on an anisotropic polymer substrate was measured for a range of in-plane loading orientations. The layer was produced using either an isotropic sheet-to-sheet (S2S) process, or an anisotropic R2R process in order to discriminate between the respective influences of substrate anisotropy and internal stress anisotropy.

2. Materials and experimental methods

The substrate was a 50 ± 5 μm thick polyethylene terephthalate foil (PET, Melinex 401, DuPont Teijin Films) supplied in the form of a 40 cm wide roll. A 136 nm thick multilayer stack of Sn-doped In_2O_3 (ITO) and Ag (ITO 30 nm/Ag 8 nm/ITO 60 nm/Ag 8 nm/ITO 30 nm, ITOA) was deposited on the PET substrate using R2R and S2S processes. R2R depositions were carried out with a modular web-coating unit (SMARTWEB™, Applied Materials GmbH). This unit has successive independent deposition chambers that enable the deposition of

* Corresponding author. Tel.: +41 21 693 4848; fax: +41 21 693 5880.
E-mail address: yves.leterrier@epfl.ch (Y. Leterrier).

0040-6090/$ – see front matter © 2010 Elsevier B.V. All rights reserved.
doi:10.1016/j.tsf.2010.07.033

Nomenclature

A, B	parameters
COS, ε_{onset}	Crack onset strain
$E_1 = E_3$, E_2	Young's moduli of the transversely isotropic substrate associated with the axes of orthotropy
E_x , E_y	Young's moduli of the transversely isotropic substrate associated with the in-plane loading axes
E_c, $\bar{E}_c$	Young's modulus and plane strain modulus of the coating
G_{13}, $G_{12} = G_{23}$	shear moduli of the transversely isotropic substrate associated with the axes of orthotropy
G_{xy}	shear modulus of the transversely isotropic substrate associated with the in-plane loading axes
G_{ss}	steady-state energy release rate of a channeling crack in the coating
G_{Ic}	mode I critical energy release rate
g_1, g_2	non-dimensional steady-state energy release rates of a channeling crack in the coating running in transverse and machine directions, respectively
h	substrate thickness
h_c	coating thickness
R_{iu}, R_{ic}	radius of curvature of the uncoated and coated substrates, respectively along MD ($i=1$) and TD ($i=2$)
α, β	Dundurs' parameters
ε_x, ε_y	in plane strains, respectively parallel and transverse to the loading direction
γ_{xy}	in-plane shear strain
$\eta_{xy,x}$	coefficient of mutual influence of the second kind for the transversely isotropic substrate
ν_{12} , $\nu_{21} = \nu_{23}$	Poisson's ratios of the transversely isotropic substrate associated with the axes of orthotropy
ν_c	Poisson's ratio of the coating
ν_s	Poisson's ratio of isotropic substrate
ν_{xy}	Poisson's ratio of the transversely isotropic substrate associated with the in-plane loading axes
σ_I	first principal stress in the coating
σ_{1r}	internal stress in the coating in machine direction
σ_{2r}	internal stress in the coating in transverse direction
σ_f	coating tensile strength
σ_x^0	pre-stress in the coating in machine direction
σ_x^c, σ_y^c, σ_{xy}^c	stresses in the coating associated with the in-plane loading axes
θ	in-plane orientation angle

multilayer stacks in a single run. Deposition was carried out with RF-magnetron sputtering on the PET foil moving on a drum, with an initial base pressure of approximately 10^{-5} Pa. The temperature of the coating drum was −10 °C, and the substrate temperature during deposition was estimated from previous experience to be 20 °C. A tensile line load equal to 357 N/m was applied to the PET foil in the machine direction (MD). Upon release of the load and elastic recovery of the substrate, the coating should experience a compressive strain along MD equal to approximately 0.17%, which will be added to other sources, such as thermal and intrinsic strains [17]. In fact the actual strain anisotropy in the foil at the sputter location was not analyzed, since part of the tensile load was transferred through friction between the substrate and the rolls. As will be discussed below, the coating stress state determined from the analysis of film curvature before and after coating deposition was not consistent with the critical strain data. This was thought to result from changes in substrate curvature during R2R processing. In order to check this, the foil was processed in the R2R unit without deposition taking place. This will henceforth be referred to as 'R2R processed PET'. S2S depositions were carried out with an in-line sputter coater unit (Aristo 1200, Applied Materials GmbH). A rectangular sample was cut from the PET foil and was attached to a 0.5 m × 0.4 m glass carrier plate, which was exposed and moved facing the sputtering cathodes. The temperature increase during S2S depositions was comparable to that of the R2R process, although cooling of the sheet was not as effective as that obtained with the cooling drum. In fact, the sputter parameters were adapted for the S2S depositions without changing the properties of the deposited films (transparency and conductivity). This was achieved by reducing the applied power density (1/10 of the power in the R2R process). The temperature of the carrier after the coating runs was not measured, but was estimated to be approximately 40 °C. Prior to further testing, both uncoated and R2R coated substrates were kept on their rolls of similar diameter, and S2S samples were kept attached to their carrier plate, all in exactly the same ambient conditions.

The principal axes of the in-plane anisotropy problem are sketched in Fig. 1. Axis 1 is parallel to the PET roll radius with an in-plane angle $\theta = 0°$ (MD). Axis 2 is parallel to the width of the roll with $\theta = 90°$ (transverse direction, TD). Axis 3 (not shown in the figure) is normal to the plane of the PET foil. The principal directions of the elasticity tensor were assumed to coincide with the optical axes. They were determined from the measured optical extinction of the film, observed under cross-polarizers, and found to coincide with the MD and TD within 5°.

The Young's modulus of the PET and R2R processed PET substrates was measured using tensile testing. Rectangular specimens of gauge dimensions equal to 25 mm × 250 mm were cut from the foils along $\theta = 0°$, 30°, 45°, 60° and 90° directions, and tested at room temperature under a constant nominal rate equal to $3.3 \times 10^{-4}\ s^{-1}$ using a tensile frame apparatus (UTS Testsystem). The Poisson's ratio

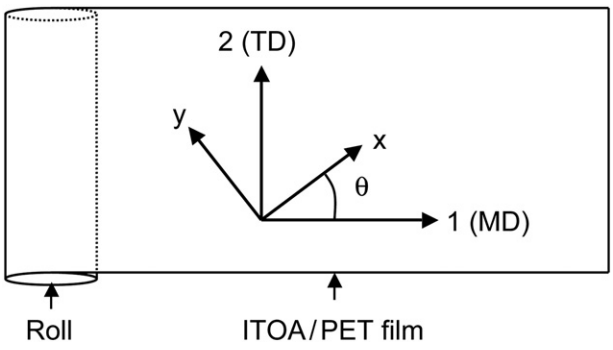

Fig. 1. Definitions of in-plane orientations in the ITOA/PET film.

of the PET and R2R processed PET substrates was determined using tensile tests carried out *in-situ* in an optical microscope (Olympus BX60) equipped with a miniature tensile frame (Minimat, Rheometric System). Rectangular samples with gauge dimensions equal to 5.5 mm × 40 mm were cut from the foils along MD and TD. A series of 100 μm-diameter ink dots were carefully drawn along the sample length and width directions for video-extensometry purposes. Micrographies taken at 50× magnification were captured, using a charge coupled device camera, and processed using a digital image analysis tool (Analysis, SIS). The Poisson's ratio was calculated from the relative displacement between the center of gravity of individual dots, perpendicular to the loading direction.

The ITOA coating was in-plane isotropic, as indicated by resistivity measurements and atomic force microscopy analysis. Its Young's modulus E_c and Poisson's ratio ν_c were estimated from values for ITO films (modulus 119 GPa obtained from nano-indentation tests, and Poisson's ratio assumed to be equal to 0.2) and Ag (modulus 83 GPa and Poisson's ratio 0.37) using the rule of mixtures and was found to be equal to 114 GPa and 0.22, respectively.

Fragmentation tests were carried out under uniaxial loading to determine the COS of the ITOA coating. In this test the development of crack patterns was analyzed as a function of strain *in-situ* in a microscope in order to resolve the damage state in layers with sub-micrometer thickness [18,19]. Rectangular samples, of gauge length equal to either 16 mm or 40 mm and width equal to 5.5 mm, were carefully cut from the foils along $\theta = 0°$, 30°, 45°, 60° and 90° directions using a scalpel. Tests were carried out at a nominal strain rate equal to 4.2×10^{-4} s^{-1} *in-situ* in an optical microscope, using the same set-up as for the Poisson's ratio measurements. Three different preloads were tested: 0, 1 and 4 N (corresponding to pre-stress levels equal to 0, 3.6 and 14.4 MPa). A Linkam miniature tensile frame (TST-350) was used for the 0 and 1 N preload experiments (using samples of gauge length equal to 16 mm), and the Minimat frame was used for the 4 N preload (using samples of gauge length equal to 40 mm). The coating strain at failure was measured with an accuracy better than 10^{-3}. The progressive cracking of the coating was analyzed in terms of crack density (CD), equal to the number of tensile cracks per unit length multiplied by substrate elongation to correct to a first approximation for crack opening. The COS was determined from a linear extrapolation of the crack density *vs.* strain data, in the early fragmentation stages. The COS corresponded to the onset of unstable propagation of cracks, as will be confirmed below. At least two samples of each type of film were analyzed, and the reported COS data were averaged over the number of tested samples.

The process-induced internal stress in the ITOA coating, σ_{ir}, was determined along MD ($i = 1$) and TD ($i = 2$) from radius of curvature measurements on 60×5.5 mm^2 rectangular samples, following the analysis of Röll [20]:

$$\sigma_{ir} = -\frac{E_i h^2}{6(1-\nu_i)h_c}\left(1 + \frac{h_c}{h}\left(4\frac{E_c}{E_i} - 1\right)\right)\cdot\left(\frac{1}{R_{ic}} - \frac{1}{R_{iu}}\right) \quad (1)$$

where E_i and ν_i are the Young's modulus and Poisson's ratio of the substrate along MD ($i = 1$) and TD ($i = 2$), E_c is the Young's modulus of the ITOA coating, h and h_c are the thicknesses of the substrate and coating, respectively, and R_{iu} and R_{ic} are the radii of curvature of the uncoated and coated substrates, respectively. The usual convention, where compressive stresses are negative, was adopted. Accounting for the in-plane deformations (e.g., [21]) would reduce the calculated stresses by less than 1% compared to the values reported below, and the sample curvature was low enough so that more complicated non-linear geometry calculations [22] were not necessary. As will be detailed below, the curvature of the polymer substrate itself changed during coating processing, which added to curvature changes resulting from the build-up of internal stresses, and the value of R_{iu} was left as an adjustable parameter.

3. Experimental results

3.1. Substrate anisotropy

Figs. 2 and 3 show the Young's modulus and Poisson's ratio of the as-received and R2R processed PET substrates as a function of in-plane orientation. The experimental data are compared with theoretical values, as detailed in the following sections. The properties of the R2R processed foil were very similar to those of the as-received foil. In both cases a marked anisotropy was evident, with a 35% increase of Young's modulus from MD to TD. This reflected the process-induced molecular orientation state of the polymer and confirmed previous analyses [9–11].

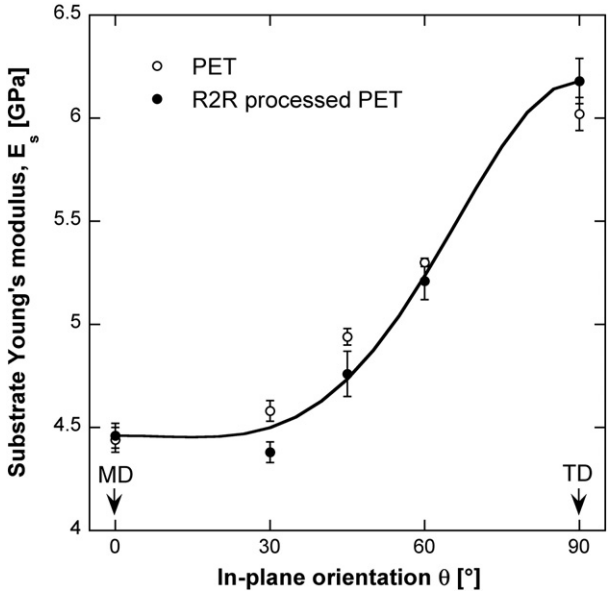

Fig. 2. Young's modulus of the PET substrate as a function of in-plane orientation. The curve represents Eq. (2).

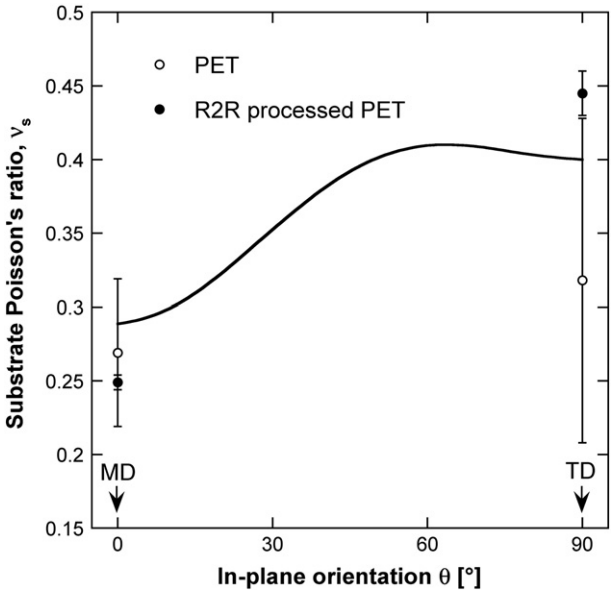

Fig. 3. Effective Poisson's ratio of the PET substrate as a function of in-plane orientation. The curve represents Eq. (3).

3.2. Cracking anisotropy

Fig. 4 shows the tensile damage state in the ITOA coating for both S2S and R2R films loaded along the MD and the TD to the same 1.1% strain. Cracks were present in all cases, with the notable exception of the R2R film loaded along the MD. The absence of cracks in the latter case motivated the present study, and the reasons for this exception are discussed below. Cracks were initiated on coating defects, as shown in several micrographs in the figure. Cutting samples from the foil produced edge defects in the coating, also likely to initiate cracks. It in fact became evident that process-induced defects such as pinholes were more critical than edge defects, and most cracks initiated from process-induced defective sites. This was clearly established in a recent study of ITO coatings on polymers, where ITO lines with smooth edges deposited through a mask had the same propagation strain (i.e., COS) as continuous ITO coatings with cutting edge defects [23]. It was, moreover, ascertained that, in the early cracking stages, cracks propagated in the coating and not at the coating/substrate interface, as revealed by the absence of delamination along the edges of coating fragments. Crack propagation in the substrate could also be excluded (see the end of the present section).

Fig. 5 shows the density of tensile cracks in the ITOA coating *vs.* strain with a 4 N preload, in the case of the S2S film and for a range of loading orientations θ. The COS was close to 1% for all directions, and appeared to be slightly higher for $\theta = 45°$. These COS data are reported in Fig. 6, together with the data for films without preloading and with a 1 N preload, and compared with the theoretical values. One can see that, as expected, the higher the preload, the lower the COS. The COS along MD was equal to that along TD within experimental scatter. This result was consistent with isotropic S2S processing conditions, but not

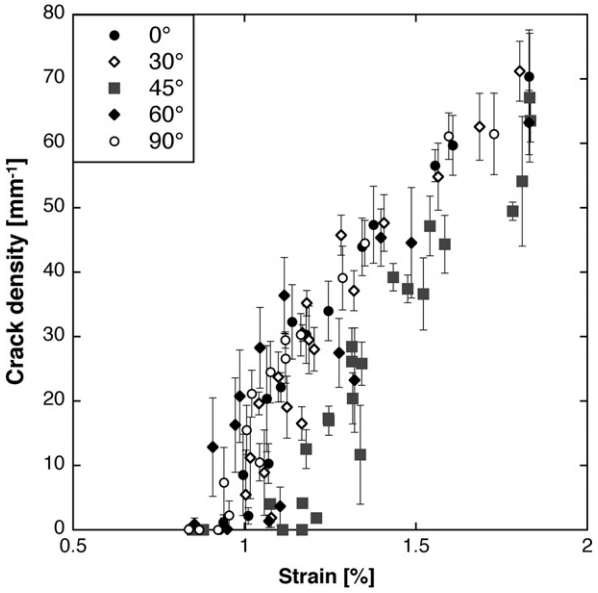

Fig. 5. Crack density *vs.* strain for S2S processed ITOA coatings on PET at different in-plane loading orientations.

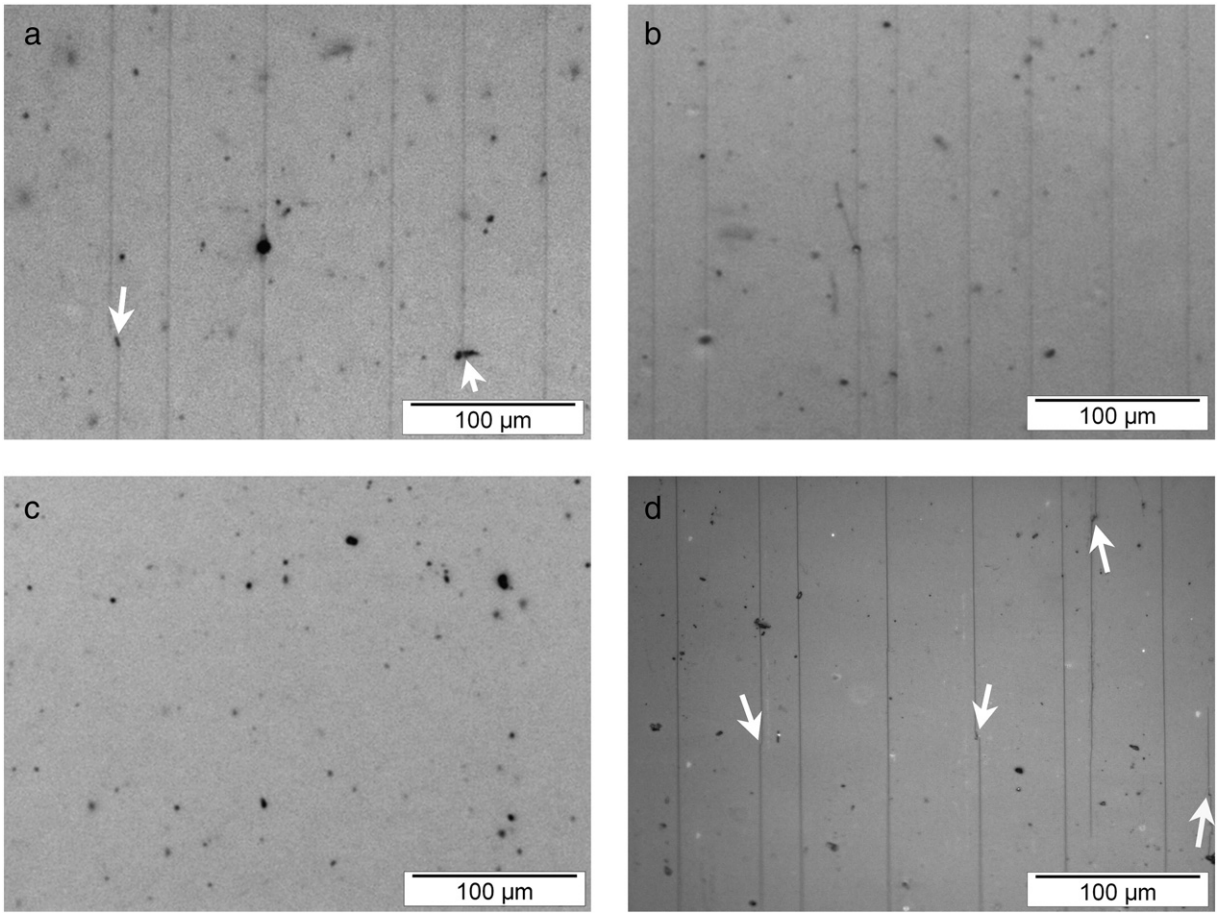

Fig. 4. Influence of process and substrate anisotropy on the damage state in the ITOA coating on PET under 1.1% strain (a: S2S film loaded along MD; b: S2S film loaded along TD; c: R2R film loaded along MD; and d: R2R film loaded along TD). The loading direction was parallel to the scale bar in the micrographs. Cracks are evident in all cases except for the R2R film loaded along MD. The arrows indicate defect initiation sites.

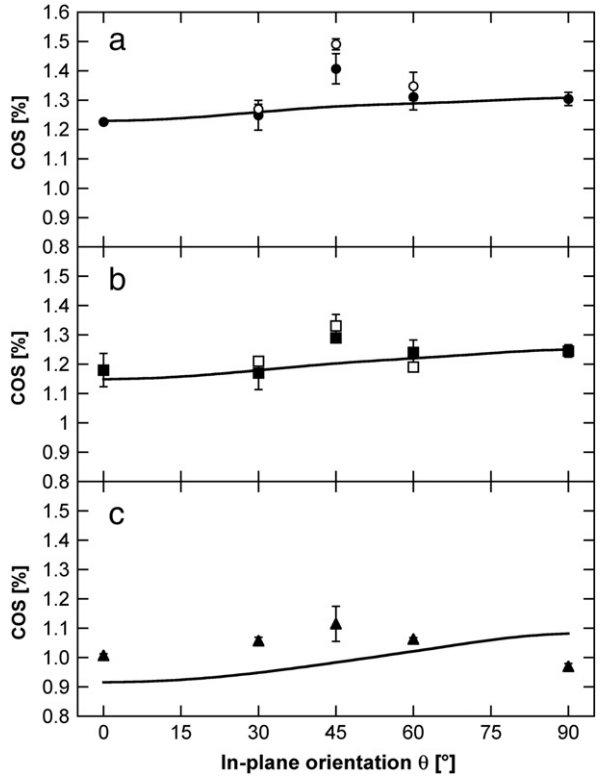

Fig. 6. COS variation with in-plane loading angle θ for S2S films with no preload (a) and with 1 N (b) and 4 N (c) preloads during fragmentation testing. Black and open symbols are for positive and negative θ values, respectively. The curves represent Eq. (19), with factors A and B given by Eq. (13).

with an anisotropic substrate, which suggested that the latter had a marginal influence on coating cracking, as will be confirmed in Section 4. The surprise came from the 45° data, with a COS systematically higher than those for other orientations. Tests were repeated, including samples cut at −30°, −45° and −60° and the same results were obtained, as shown in the figure.

Fig. 7 shows the density of tensile cracks in the ITOA coating *vs.* strain with a 4 N preload in the case of the R2R film and for a range of

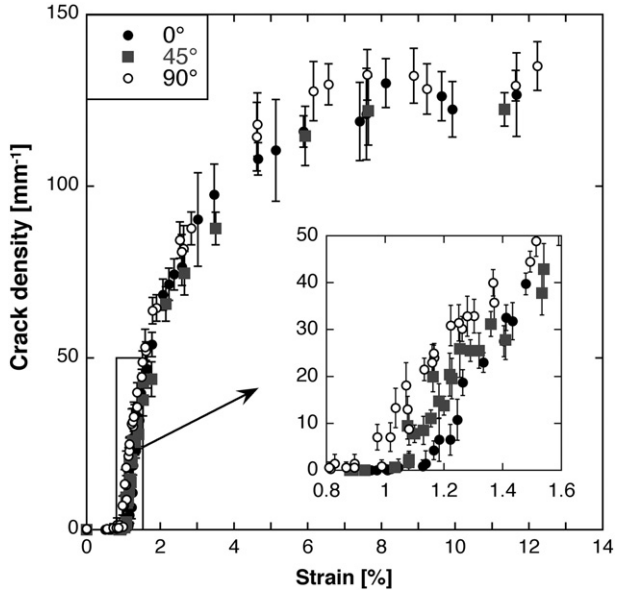

Fig. 7. Crack density *vs.* strain for R2R processed ITOA coatings on PET at different in-plane loading orientations.

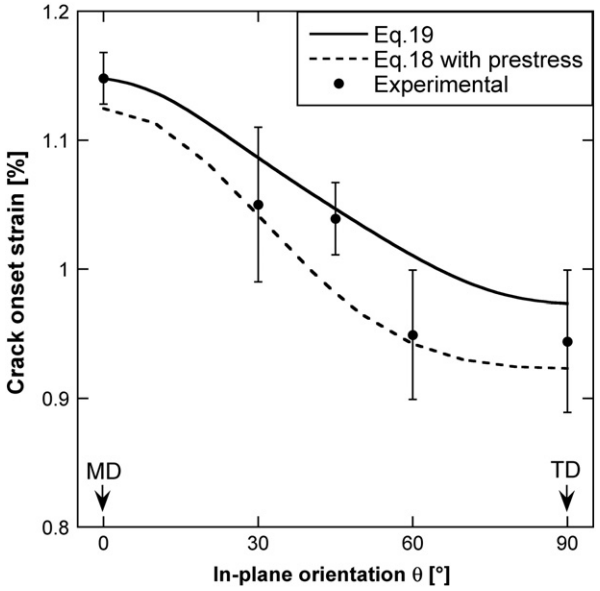

Fig. 8. COS variation with in-plane loading angle θ for R2R films with a 4 N preload during fragmentation testing. Eq. 18 including pre-stress (isotropic substrate and same Poisson's ratio for coating and substrate) and Eq. 19 (anisotropic substrate and different Poisson's ratio for coating and substrate) are compared with experimental data.

loading orientations θ. As shown in Fig. 8, the COS decreased from 1.15% along MD to 0.94% along TD. This COS difference of *ca.* 0.2% matched the calculated pre-strain of 0.17% resulting from the tensile loading of the foil during processing. This value was also consistent with data for a 25 μm thick PET foil loaded to 180 N/m in R2R processing units, with pre-strain reported to be around 0.15% [8]. The average of the COS values at 45° seemed to be higher than would have been expected when looking at the data obtained at other orientations; however, experimental scatter was too high to draw further conclusions.

As shown in Fig. 7, the crack density at saturation of the fragmentation process was found to be equal to approximately 130 mm^{-1}. This reflected a very effective stress transfer from the substrate to the coating, i.e., good interfacial adhesion. The interfacial shear strength derived from a Kelly–Tyson analysis (see [24]) was found to be equal to 40.2 ± 2.9 MPa. This value compares with the shear stress at yield τ_Y of the PET substrate equal to 50.8 MPa (the latter value was calculated from the measured tensile stress at yield of the R2R processed PET foil, σ_Y, equal to 88 MPa using the Von Mises criteria: $\tau_Y = \sigma_Y / \sqrt{3}$). Such adhesion levels prevented delamination in the early fragmentation stages. Delamination eventually developed beyond 10% strain, which could be seen both from Fizeau interference patterns along fragment edges, and from transverse buckling instabilities controlled by Poisson's ratio effects. The occurrence of interfacial cracks would exclude cracks penetrating into the substrate. In fact, the strain at break of the ITOA/PET film was as high as that in the uncoated PET film, which would not have been possible if coating cracks had propagated into the PET.

3.3. Internal strain anisotropy

The radius of curvature of the film specimens and corresponding process-induced internal stresses in the ITOA coating are reported in Table 1. The as-received PET substrate was almost flat with a radius of curvature close to 1 m along MD, and close to 4 m along TD. In contrast, the S2S coated samples were curved, as a result of process-induced stresses. Samples cut along the MD, TD and +45° orientation are shown in Fig. 9. Along the MD and TD, the curvatures were 1D homogeneous, which allowed a direct measurement of the radii of curvature. A marked anisotropy was also evident, the curvature being more pronounced

Table 1
Radius of curvature and internal stress in R2R and S2S processed ITOA coatings on PET along the MD ($\theta = 0°$) and the TD ($\theta = 90°$).

Material	θ (°)	Radius of curvature [mm]	Internal stress in coating (Eq. 1) [MPa]		
			Using as-received PET radius	Using R2R processed PET radius	Compatible with COS data
PET	0	1080 ± 430	–	–	–
	90	4300 ± 3500	–	–	–
R2R processed PET	0	246 ± 21	–	–	–
	90	1360 ± 400	–	–	–
R2R ITOA/PET	0	19.7 ± 1.0	−1160	−1080	−430
	90	380 ± 80	−98	−77	−98
S2S ITOA/PET	0	32.4 ± 4.5	−695	–	−155
	90	191 ± 95	−204	–	−204

along the MD compared to the TD. This was unexpected, since the deposition conditions were isotropic, and was therefore checked, using samples of different geometries, in order to verify that the anisotropy was not a consequence of bifurcation phenomena in the curvature of thin plates [22]. The 45° samples twisted with a significant helical curl, a consequence of curling in one of the principal directions. The in-plane stress in the ITOA coating along MD and TD, calculated by using the measured radii before and after deposition (Eq. 1), was found to be compressive and indeed highly anisotropic, being equal to 700 MPa and 200 MPa along MD and TD, respectively.

The R2R processed films exhibited a pronounced curvature anisotropy, with a radius as low as 2 cm along MD. The corresponding compressive stress was equal to 1.2 GPa. This value appears to be somewhat unrealistic, and such a high stress may have relaxed through wrinkling or buckling instabilities, which did not occur. It also corresponds to a compressive strain of approximately 1%, which implies that the intrinsic strain-to-failure of the ITOA coating (actual COS corrected for the internal strain) would then be close to 0, which is also quite doubtful. In addition, in both R2R and S2S cases the stress state was not consistent with the COS data. The COS difference between MD and TD was equal to 0.2% for the R2R films. With a modulus of 114 GPa, this difference corresponds to a stress difference of 228 MPa, which does not match the internal stress difference of approximately 1 GPa. The same goes for the S2S case. One may disregard here the minor influence of substrate anisotropy, as will be detailed in the next section, so that other factors must be invoked.

In order to clarify this problem, the curvature of the R2R processed PET was included in the analysis of the R2R processed films. It was found to increase significantly for both MD and TD compared to the as-received foil. The curvature radius remained larger than 1 m along TD, but was reduced to 25 cm along MD. No attempt was made to identify the origin of this change of curvature, which was assumed to result from annealing and creep phenomena when the foil was moved and conformed on the process rolls. Such an anisotropic shape memory phenomenon is rather common in polymer films. It is primarily the consequence of visco-elastic relaxation processes in the initially pre-stretched film [25–27], and

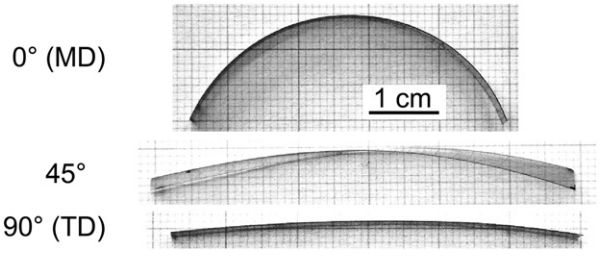

Fig. 9. Photographs of S2S processed ITOA/PET film samples along MD ($\theta = 0°$) and TD ($\theta = 90°$), and at a 45° orientation.

was reported to directly influence the internal stress and COS of silica coatings on PET [28]. It may be prevented by using heat-stabilized substrates [29]. The ITOA coating stress of the R2R samples was recalculated using these new radii values. The data reported in Table 1 are still inconsistent with the COS data, although to a lesser extent compared to the previous set of stress data. The likely reason is that the R2R processed PET was loaded in the R2R equipment without deposition taking place, hence it did not experience any deposition-induced structural changes. It was therefore decided to leave the internal stress along MD as an adjustable parameter in the following analysis.

The interplay between substrate anisotropy, internal stress anisotropy and cracking anisotropy is examined in the following section, starting with the S2S case with different pre-stress levels during fragmentation testing, and paying special attention to the 45° anomaly.

4. Fracture mechanics analysis of crack onset strain

4.1. Elastic parameters

The orthotropic R2R processed PET substrate was selected for analysis. It was modeled as a transversely isotropic material with respect to axis 2 (i.e., 1–3 is the isotropy plane) so that $\nu_{21} = \nu_{23}$, $E_1 = E_3$, and $G_{12} = G_{23}$. Accounting for the small difference in the orientation (less than 5°) between the principal directions and the MD and TD would complicate the analysis with little change in final results. Such a simplifying assumption of transverse isotropy is validated by the experimental results [9,10] demonstrating that the through-thickness modulus, E_3, is close, if not coinciding, to the smaller of the principal in-plane moduli, E_1, of the film. The compliance of a transversely isotropic material under plane stress conditions is given as [10]:

$$\frac{1}{E_x} = \frac{\cos^4\theta}{E_1} + \frac{\sin^4\theta}{E_2} + \left(\frac{1}{G_{12}} - \frac{2\nu_{12}}{E_1}\right)\sin^2\theta\cos^2\theta \tag{2}$$

with $\nu_{12}/E_1 = \nu_{21}/E_2$. A similar expression relates Poisson's ratio in specimen axes to the substrate elasticity parameters in principal axes [10]. Thus:

$$\nu_{xy} = E_x\left[\frac{\nu_{12}}{E_1}\left(\sin^4\theta + \cos^4\theta\right) - \left(\frac{1}{E_1} + \frac{1}{E_2} - \frac{1}{G_{12}}\right)\sin^2\theta\cos^2\theta\right]. \tag{3}$$

Eqs. (2) and (3) were fitted to the experimental data using $E_1 = 4.46$ GPa and $E_2 = 6.18$ GPa, and the results are shown in Figs. 2 and 3, giving $G_{12} = 1.69$ GPa and $\nu_{12} = 0.29$. These values are very close to values obtained and reported for a variety of methods [9–11].

4.2. Numerical analysis of the influence of substrate anisotropy

The energy release rate (ERR) associated with the channeling propagation of a coating crack is a function of the elastic mismatch of the coating and substrate [30] (and also, generally, substrate thickness [31]). Therefore, the elastic anisotropy of the substrate should lead to a variation of ERR of a coating crack depending on the direction of its growth. In order to evaluate the magnitude of this effect, the ERR for a mode I crack propagating along the directions of the largest and smallest stiffness of the substrate was compared. When a tensile load is applied along one of the principal in-plane directions of the transversely isotropic PET substrate, the mechanics of coating cracking are not qualitatively affected by substrate anisotropy because there are no couplings, e.g. extension–shear coupling, under such loads. Therefore, the steady-state ERR can be represented, in a form suggested in [30] for mode I crack, as:

$$G_{ss} = \frac{\pi}{2}\frac{\sigma_i^2 h_c}{\bar{E}_c} g_i \tag{4}$$

where $i=1, 2$ designates loading axis and $g = g\left(\alpha, \beta, \frac{h_c}{h}\right)$ is a non-dimensional ERR function of Dundurs' parameters α and β and, generally, of coating and substrate thickness ratio. The non-dimensional ERR, g, depends on the loading direction, $g_1 \neq g_2$, due to anisotropy of the substrate. Note that coating toughness can be evaluated by Eq. (4), as G_{ss} at crack onset stress. The applicability conditions for such an estimate were discussed in [32], and were validated in the present case with cracks of sufficient length at propagation onset (see Fig. 4).

2D plane strain finite element modeling (FEM) by a commercial code ABAQUS, accounting for the finite thickness and elastic anisotropy of the substrate, produced $g_1 = 6.17$ and $g_2 = 5.52$. It shows that the anisotropy of ERR is moderate, with $g_1/g_2 = 1.12$. It follows from Eq. (4) that the coating stress at crack onset in the isotropic coating is inversely proportional to the square root of g, hence the ratio of critical stresses in the principal directions caused by the elastic anisotropy of the substrate is $\sqrt{g_1/g_2} = 1.06$. Thus anisotropy of the non-dimensional ERR has only a minor effect on COS, and will be disregarded in further analysis.

Having determined the non-dimensional ERRs, the minimum length of a coating flaw for which steady-state cracking conditions apply can be estimated, based on the numerical models of the dependence of crack driving force on crack length as reported in [33,34]. According to a more conservative estimate, the steady-state limit is, approximately, $\frac{3}{2}\pi h_c g$ [34]. In the present case, it transpires that the coating cracks of a length exceeding 4 μm were under steady-state conditions and their ERR is given by Eq. (4).

4.3. Anisotropic stress analysis

The following stress analysis was developed assuming that the principal axes of coating internal stresses coincide with the orthotropy axes of the substrate. The analysis considers a coating/substrate film subjected to uniaxial in-plane tension at an angle θ to the orthotropy axis 1 of the substrate. Disregarding the influence of the thin coating on the mechanical response of the composite film, the strains in the film along the loading direction (x) and transverse to it (y) were determined as:

$$\varepsilon_x = \frac{\sigma}{E_x};\ \varepsilon_y = -\nu_{xy}\varepsilon_x \tag{5}$$

where σ is the applied stress and the elasticity parameters E_x and ν_{xy} are given by Eqs. (2) and (3). Due to anisotropy of the substrate, the tensile load induces an in-plane shear strain

$$\gamma_{xy} = \eta_{xy,x}\varepsilon_x \tag{6}$$

where the coefficient of mutual influence of the second kind, $\eta_{xy,x}$, is given by [35,36]:

$$\eta_{xy,x} = E_x\left[\left(\frac{2}{E_2} + \frac{2\nu_{12}}{E_1} - \frac{1}{G_{12}}\right)\sin^3\theta\cos\theta - \left(\frac{2}{E_1} + \frac{2\nu_{12}}{E_2} - \frac{1}{G_{12}}\right)\sin\theta\cos^3\theta\right]. \tag{7}$$

Having thus determined the strains in the film (Eqs. 5 and 6), the stresses in the isotropic coating under plane stress conditions due to mechanical load are expressed as:

$$\sigma_x^c = \frac{E_c\left(1-\nu_c\nu_{xy}\right)}{1-\nu_c^2}\varepsilon_x;\ \sigma_y^c = \frac{E_c\left(\nu_c-\nu_{xy}\right)}{1-\nu_c^2}\varepsilon_x;\ \sigma_{xy}^c = \frac{E_c\eta_{xy,x}}{2(1+\nu_c)}\varepsilon_x. \tag{8}$$

Accounting for the internal stresses in the coating with principal values σ_{1r} and σ_{2r}, respectively, then by adding the mechanical and internal contributions to the stress state one finally obtains:

$$\begin{aligned}
\sigma_x^c &= \frac{E_c\left(1-\nu_c\nu_{xy}\right)}{1-\nu_c^2}\varepsilon_x + \sigma_{1r}\cos^2\theta + \sigma_{2r}\sin^2\theta \\
\sigma_y^c &= \frac{E_c\left(\nu_c-\nu_{xy}\right)}{1-\nu_c^2}\varepsilon_x + \sigma_{1r}\sin^2\theta + \sigma_{2r}\cos^2\theta \\
\sigma_{xy}^c &= \frac{E_c\eta_{xy,x}}{2(1+\nu_c^c)}\varepsilon_x - (\sigma_{1r}-\sigma_{2r})\sin\theta\cos\theta.
\end{aligned} \tag{9}$$

4.4. Crack onset stress and strain analysis

The coating is under a combined plane stress loading (Eq. 9) and its failure (i.e., channeling crack propagation) is controlled by a critical energy release rate. Coating microcracks oriented normal to the first principal stress, σ_I, are most heavily loaded, hence most likely to act as initiation sites for channeling cracks. It has, moreover, been established that cracks tend to orient so that they propagate perpendicularly to the principal (tensile) stress direction in an isotropic body. Thus σ_I governs cracking of the coating. Elementary transformations yield maximum principal stress for the loading under consideration as:

$$\sigma_I = \frac{1}{2}\left(\sigma_{1r} + \sigma_{2r} + \frac{E_c\left(1-\nu_{xy}\right)}{1-\nu_c}\varepsilon_x + \sqrt{(\sigma_{1r}-\sigma_{2r})^2 + \left(\frac{E_c\varepsilon_x}{1+\nu_c}\right)^2\left(\eta_{xy,x}^2 + \left(1+\nu_{xy}\right)^2\right) + 2\frac{E_c\varepsilon_x}{1+\nu_c}(\sigma_{1r}-\sigma_{2r})\left(\left(1+\nu_{xy}\right)\cos 2\theta - \eta_{xy,x}\sin 2\theta\right)}\right). \tag{10}$$

The criterion for crack onset is $\sigma_I = \sigma_f$, where the fracture stress for a brittle coating is determined by Finite Fracture Mechanics considerations. Hence:

$$\sigma_f = \sqrt{\frac{2}{\pi}\frac{G_{Ic}\bar{E}_c}{h_c g}} \tag{11}$$

where $\bar{E}_c = E_c/\left(1-\nu_c^2\right)$ denotes the plane strain modulus of the coating and G_{Ic} is the mode I critical energy release rate of the coating. Note that the effect of the elastic anisotropy of the substrate on propagation of the coating crack, *via* e.g. directional dependence of g and mode mixity, is hereby disregarded, and σ_f is assumed not to depend on the direction of crack propagation.

Inserting Eq. (10) into the crack onset criterion $\sigma_I = \sigma_f$ and solving for the applied strain, one obtains:

$$\varepsilon_x = \frac{1-\nu_c^2}{E_c}\ \frac{-A \pm \sqrt{A^2 + 4B\left(\sigma_f-\sigma_{1r}\right)\left(\sigma_f-\sigma_{2r}\right)}}{B} \tag{12}$$

with

$$A = \left(2\sigma_f - \sigma_{1r} - \sigma_{2r}\right)(1+\nu_c)\left(1-\nu_{xy}\right) + (\sigma_{1r} - \sigma_{2r})(1-\nu_c)\left(\left(1+\nu_{xy}\right)\cos 2\theta - \eta_{xy,x}\sin 2\theta\right) \quad (13a)$$

$$B = \left(\eta_{xy,x}(1-\nu_c)\right)^2 - 4\left(\nu_c - \nu_{xy}\right)\left(1-\nu_c\nu_{xy}\right). \quad (13b)$$

The directional dependence of the COS, ε_{onset}, is given by the positive root in Eq. (12):

$$\varepsilon_{onset}(\theta) = \frac{1-\nu_c^2}{E_c}\frac{-A + \sqrt{A^2 + 4B\left(\sigma_f - \sigma_{1r}\right)\left(\sigma_f - \sigma_{2r}\right)}}{B}. \quad (14)$$

Eqs. (13) and (14) simplify somewhat for an isotropic substrate for which $E_x = E_s$, $\nu_{xy} = \nu_s$, and $\eta_{xy,x} = 0$. If $\nu_c \neq \nu_s$ (Poisson's ratios of substrate and coating differ), COS is given by Eq. (14) with the parameters:

$$A = (1+\nu_c)(1-\nu_s)\left[2\sigma_f - \sigma_{1r} - \sigma_{2r} + (\sigma_{1r} - \sigma_{2r})\cos 2\theta\right] \quad (15a)$$

$$B = -4(\nu_c - \nu_s)(1-\nu_c\nu_s). \quad (15b)$$

However, when $\nu_c = \nu_s$ (i.e., Poisson's ratios of substrate and coating are equal) then:

$$A = \left(1-\nu_c^2\right)\left[2\sigma_f - \sigma_{1r} - \sigma_{2r} + (\sigma_{1r} - \sigma_{2r})\cos 2\theta\right] \quad (16a)$$

$$B = 0 \quad (16b)$$

and the COS is determined as the limit of the right-hand-side of Eq. (14) at $B \to 0$. Therefore

$$\varepsilon_{onset}(\theta) = \lim_{B\to 0}\frac{1-\nu_c^2}{E_c}\frac{-A + \sqrt{A^2 + 4B\left(\sigma_f - \sigma_{1r}\right)\left(\sigma_f - \sigma_{2r}\right)}}{B} = \frac{1-\nu_c^2}{E_c}\frac{4\left(\sigma_f - \sigma_{1r}\right)\left(\sigma_f - \sigma_{2r}\right)}{2|A|} \quad (17)$$

leading to

$$\varepsilon_{onset}(\theta) = \frac{2}{E_c}\frac{\left(\sigma_f - \sigma_{1r}\right)\left(\sigma_f - \sigma_{2r}\right)}{2\sigma_f - \sigma_{1r} - \sigma_{2r} + (\sigma_{1r} - \sigma_{2r})\cos 2\theta}. \quad (18)$$

Finally, if a pre-stress σ_x^0 is applied before mechanical loading, and for the general case of an anisotropic substrate and different Poisson's ratio for coating and substrate, Eq. (14) is rewritten using parameters A and B given by Eq. 13 as:

$$\varepsilon_{onset}(\theta) = \frac{1-\nu_c^2}{E_c}\frac{-A + \sqrt{A^2 + 4B\left(\sigma_f - \sigma_{1r}\right)\left(\sigma_f - \sigma_{2r}\right)}}{B} - \frac{\sigma_x^0}{E_x}. \quad (19)$$

4.5. Comparison with test results for S2S films

Fig. 6 compares Eq. (19) with experimental data for the three levels of pre-stress. The coating tensile strength σ_f was calculated first using the COS along TD with zero pre-stress, and the internal stress also along TD as $\sigma_f = \frac{E_c(1-\nu_c\nu_{21})}{1-\nu_c^2}\varepsilon_{onset}(90^\circ) + \sigma_{2r}$ and found to be equal to 1220 MPa. The internal stress along MD was then fitted to the measured COS along that direction, and found to be equal to −155 MPa. This value is approximately four times lower than the values derived using the measured substrate curvature radius (Table 1), and this discrepancy was thought to result from the change of substrate curvature during processing. The radius of curvature of the uncoated substrate, which is compatible with an internal stress equal to −155 MPa according to Eq. (1), is equal to 4.1 cm. This value is representative of roll radius dimensions, which would be consistent with the previously mentioned curvature effect. The coating critical energy release rate was obtained using Eq. (11) and the value of g_2 as determined in Section 4.2, thus leading to $G_{Ic} = 14.7$ J/m^2.

With the values of coating strength and internal stress established for the reference case with 0 preload, the model was then compared with the data obtained for the 1 and 4 N preload levels. The theoretical results shown in Fig. 6b and c accurately reproduce the 1 N preload data, but are less precise for the 4 N preload data. This is probably due to the limited accuracy of the load cell attached to the Minimat frame. Nevertheless, the model is able to reproduce the measured COS for given preload levels — except at a 45° orientation.

4.6. The 45° anomaly

The origin of the discrepancy between the experimental S2S data and the model values in the case of the 45° orientation is discussed below, based on various assumptions which relate to the morphology and the mechanical properties of the PET substrate and of the coating layer. First of all, it was verified that the applied strain rate was correctly controlled during the experiments for all orientations, so that visco-elastic effects due to the straining of the PET substrate could be disregarded. Then, localized, patterned and/or directional variations of the thickness of the coating layer were considered. Based on the anisotropic model developed in the previous section, and on the average value of COS at a 45° orientation, the first principal stress σ_I was found to be equal to 1.41 GPa. With an energy release rate $G_{Ic} = 14.7$ J/m^2 and using Eq. (11) one obtains an 'effective' thickness of the coating layer along the 45° orientation of about 90 nm, which is much less than the expected 136 nm. The corresponding thickness difference of 46 nm is not consistent with the root mean square roughness of the ITOA coating as measured over a 2 μm × 2 μm area using atomic force microscopy and found to be equal to 1.14 nm. Thus, a variation of coating thickness is not the right explanation to account for the observed increase of COS at a 45° orientation. It was then postulated that the COS increase might be related to extension–shear coupling in the composite ITOA/PET film. Nevertheless, this effect has a negligible influence on the COS. The angular difference between the direction of the first principal stress σ_I and the loading axis for the 45° case was found to be small and close to 4° using the previous model and FEM simulations.

Another explanation for the 45° orientation result could be related to long-scale variations in the elastic properties of the PET substrate. A new series of tensile experiments were carried out using samples cut at random locations along the PET foil with the same in-plane orientations as the samples described in Section 2. The Young's modulus along MD and TD was found to be the same, within experimental scatter, as the values shown in Fig. 2. In contrast, rather astonishing changes compared to the data given in Fig. 2 were obtained at other orientations. A modulus as high as 6.7 GPa was measured at a 45° orientation, i.e., 40% higher than the value reported in Fig. 2. The origin of such variations should be sought in terms of fluctuations of the PET lamination process, and in fact, higher PET modulus values at off-axis orientations were already reported by Blumentritt (e.g. [37]). Higher Young's modulus of the substrate would imply a lower non-dimensional ERR available for a coating crack, and therefore a higher COS at comparable internal stress in qualitative agreement with the observations at 45° loading. This implies that the long-scale variations of the elastic properties of the PET substrate do indeed contribute to the measured in-plane variations of coating critical strain, although this effect remains small, as was detailed in Section 4.2.

4.7. Comparison with test results for R2R films

Fig. 8 compares the theoretical COS (Eq. 19) with the experimental data obtained using a pre-stress equal to 14.4 MPa. The previously determined critical energy release rate equal to 14.7 J/m^2 (and related coating strength equal to 1220 MPa), and the internal stress along TD (−98 MPa) were used. As in the S2S case, the internal stress along MD was fitted to the experimental COS along MD and was found to be compressive and equal to −430 MPa. This value is much lower than those obtained using the measured substrate radius (Table 1). The substrate radius of curvature that is compatible with a stress of −430 MPa according to Eq. (1) is equal to 3.0 cm, which, again, is representative of web and roll coater dimensions. Eq. 18, corrected for the pre-stress of 14.4 MPa and using the same internal stress data (−430 MPa and −98 MPa along MD and TD, respectively) is also shown in Fig. 8. The two models reproduce most of the experimental data within scatter, which confirms the marginal influence of substrate anisotropy on anisotropic cracking of the coating. Also, the different Poisson's ratio between substrate and coating, not considered in Eq. 18, does not significantly impact on the results.

The present analysis is limited by the lack of independent determination of coating stress, and by the observed variations of in-plane elastic properties of the substrate. For crystalline coatings, X-ray and electron diffraction methods [38] would solve the coating stress problem. An alternative would be to selectively dissolve the inorganic coating and measure the resulting change of substrate curvature. These issues underline the challenge to determine the actual coating stress in the case of polymer substrates with complex structural states. In any case, increasing line load during the R2R processing of flexible devices will increase the critical coating strain along MD, which should therefore be the preferred direction for bending the device. Using highly anisotropic substrates with an enhanced molecular orientation along MD, hence an increased modulus, would be less effective, and this would be at the expense of a higher line load during R2R processing. The present investigation provides a basis for further optimizing the critical strain for the tensile failure of nano-sized coatings and device structures on flexible substrates, through the use of tailored substrates and internal stress anisotropy.

5. Conclusions

With a view to optimizing R2R processing of thin films on polymer substrates so as to ensure the mechanical integrity of flexible electronic applications, this study investigated the influence of substrate and process anisotropy on the COS of an oxide coating on PET. Isotropic S2S and anisotropic R2R processes with the same anisotropic substrate were used and the COS results were analyzed using an anisotropic stress analysis. In the S2S case the critical strain was found to be independent of orientation, except at a 45° in-plane orientation where it was 15% higher. This unexpected result was tentatively related to long-scale variations of the modulus of PET at off-axis orientations, found to be as high as 40%. In the R2R case a relative 20% increase of COS was found between TD and MD. The actual stress state along MD was unknown, but was presumably due to curvature changes of the PET substrate during coating deposition, and was instead fitted to the COS data. The influence of substrate anisotropy was found to be small, and the measured COS anisotropy was therefore primarily controlled by the internal stress anisotropy.

Acknowledgements

The authors acknowledge the EU-funded Flexidis project (IST-004354) for funding this work.

References

[1] G.P. Crawford (Ed.), Flexible Flat Panel Displays, J. Wiley, Chichester, UK, 2005.
[2] K.J. Allen, Proc. IEEE 93 (2005) 1394.
[3] R.H. Reuss, D.G. Hopper, J.G. Park, MRS Bull. 31 (2006) 447.
[4] M.C. Choi, Y. Kim, C.S. Ha, Prog. Polym. Sci. 33 (2008) 581.
[5] R. Ludwig, R. Kukla, E. Josephson, Proc. IEEE 93 (2005) 1483.
[6] Z. Suo, J. Vlassak, S. Wagner, China Particuology 3 (2005) 321.
[7] A. Pinyol, L. Rougier, D. Gilliéron, V. Mewani, Y. Leterrier, J.-A.E. Månson, P. Dumont, J. Andersons, M. Campo, P. Sauer, J. Schwenzel, 7th Annual Flexible Electronics and Displays Conference and Exhibition, Phoenix, AZ, January 21–24, 2008.
[8] C.A. Bishop, Vacuum Deposition onto Webs, Films and Foils, William Andrew Publishing, Norwich, NY, USA, 2007.
[9] Y. Okabe, N. Takeda, M. Yanaka, Y. Tsukahara, IEEE Trans. Ultrason. Ferroelectr. Freq. Control 46 (1999) 1269.
[10] R. Feng, R.J. Farris, J. Appl. Polym. Sci. 86 (2002) 2937.
[11] S.L. Zhang, J.C.M. Li, J. Polym. Sci. B. Polym. Phys. 42 (2004) 260.
[12] S.D. Cheng, Y. Zhou, C.H. Kam, W.X. Que, Y.L. Lam, Y.C. Chan, W.S. Gan, in: M. Osinski, S.J. Chua, S.F. Chichibu (Eds.), Proc. SPIE Conference on Design, Fabrication, and Characterization of Photonic Devices, Int. Soc. Opt. Eng., Singapore, 1999, p. 680.
[13] S. Lee, S.T. Choi, Y.Y. Earmme, Int. J. Sol. Struct. 43 (2006) 3401.
[14] S. Lee, S.T. Choi, Y.Y. Earmme, I Int. J. Sol. Struct. 44 (2007) 5801.
[15] S. Lee, S.T. Choi, Y.Y. Earmme, Int. J. Sol. Struct. 45 (2008) 746.
[16] X. Chen, E.K. Richman, B.L. Kirsch, R. Senter, S.H. Tolbert, V. Gupta, J. Appl. Phys. 104 (2008) 083515.
[17] P. Dumont, G. Tornare, Y. Leterrier, J.-A.E. Månson, Thin Solid Films 515 (2007) 7437.
[18] G. Rochat, Y. Leterrier, P. Fayet, J.-A.E. Månson, Thin Solid Films 437 (2003) 204.
[19] Y. Leterrier, Prog. Mater. Sci. 48 (2003) 1.
[20] K. Röll, J. Appl. Phys. 47 (1976) 3224.
[21] Y. Inoue, Y. Kobatake, Appl. Sci. Res. A7 (1958) 314.
[22] C.B. Masters, N.J. Salamon, Int. J. Eng. Sci. 31 (1993) 915.
[23] J. de Goede, P. Bouten, L. Médico, Y. Leterrier, J.-A.E. Månson, G. Nisato, in: R.P. Vinci, R. Schwaiger, A. Karim, V. Shenoy (Eds.), Stability of Thin Films and Nanostructures, Mater. Res. Soc. Symp. Proc. 854E, Warrendale, PA, 2005.
[24] Y. Leterrier, L. Boogh, J. Andersons, J.A.E. Månson, J. Polym. Sci. B. Polym. Phys. 35 (1997) 1449.
[25] B. Haworth, Z.W. Dong, P. Davidson, Polym. Int. 32 (1993) 325.
[26] R.M. Gohil, J. Appl. Polym. Sci. 48 (1993) 1635.
[27] R.M. Gohil, J. Appl. Polym. Sci. 52 (1994) 925.
[28] G. Rochat, Y. Leterrier, P. Fayet, J.A.E. Månson, Thin Solid Films 484 (2005) 94.
[29] W.A. MacDonald, M.K. Looney, D. MacKerron, R. Eveson, K. Rakos, Plast. Rubber Compos. 37 (2008) 41.
[30] J.L. Beuth, Int. J. Sol. Struct. 29 (1992) 1657.
[31] J.J. Vlassak, Int. J. Fract. 119 (2003) 299.
[32] J. Andersons, J. Modniks, Y. Leterrier, G. Tornare, P. Dumont, J.-A.E. Månson, Theor. Appl. Fract. Mech. 49 (2008) 151.
[33] Z.C. Xia, J.W. Hutchinson, J. Mech. Phys. Solids 48 (2000) 1107.
[34] J. Andersons, P.H.M. Timmermans, J. Modniks, Int. J. Fract. 148 (2007) 233.
[35] R.M. Jones, Mechanics of Composite Materials, Second Edition, Taylor & Francis, London, 1999.
[36] J.N. Reddy, Mechanics of Laminated Composite Plates and Shells: Theory and Analysis, Second Edition, CRC Press LLC publishing, Boca Raton, FL, USA, 2000.
[37] B.F. Blumentritt, IBM J. Res. Dev. 23 (1979) 66.
[38] R.P. Vinci, J.J. Vlassak, Annu. Rev. Mater. Sci. 26 (1996) 431.